



# Iterative method for large-scale Timoshenko beam models assessed on commercial-grade paperboard

Morgan Görtz<sup>1,2</sup> · Gustav Kettil<sup>1</sup> · Axel Målqvist<sup>2</sup> · Mats Fredlund<sup>3</sup> · Fredrik Edelvik<sup>1</sup>

Received: 11 December 2023 / Accepted: 15 April 2024  
© The Author(s) 2024

## Abstract

Large-scale structural simulations based on micro-mechanical models of paper products require extensive numerical resources and time. In such models, the fibrous material is often represented by connected beams. Whereas previous micro-mechanical simulations have been restricted to smaller sample problems, large-scale micro-mechanical models are considered here. These large-scale simulations are possible on a non-specialized desktop computer with 128GB of RAM using an iterative method developed for network models and based on domain decomposition. Moreover, this method is parallelizable and is also well-suited for computational clusters. In this work, the proposed memory-efficient iterative method is numerically validated for linear systems resulting from large networks of Timoshenko beams. Tensile stiffness and out-of-plane bending stiffness are simulated and validated for various commercial-grade three-ply paperboards consisting of layers composed of two different types of paper fibers. The results of these simulations show that a linear network model produces results consistent with theory and published experimental data

**Keywords** Bending · Conjugate gradient · Domain decomposition · Network · Paperboard · Timoshenko

## 1 Introduction

Wood-fiber-based materials have numerous engineering applications, with the scope expanding alongside the increased focus on sustainability. With the paper and pulp industry accounting for 6% of the global industrial energy use and 2% of direct CO<sub>2</sub> emissions [13], even minor improvements in the production of paper-based products can have substantial effects. These improvements include using more recycled paper in products, using less pulp in production, or switching to pulp with a smaller environmental footprint.

Mechanical and chemical processes are used to turn virgin wood into pulp (pulping). These processes produce different types of fiber that are suitable for different applications. For

example, kraft pulp has fine fibers from processes involving chemicals and heat that are well-suited for printing paper, whereas chemi-thermomechanical pulp (CTMP) has larger fibers that are preferable for bulk in paperboard. These differences also extend to mechanical properties in the finished products, such as sheet strength and bending stiffness [35]. Tools that provide insights into these mechanical properties can help paper product developers produce better and less resource-intensive products.

Analyses of paper-based materials are challenging because of their complex fibrous structure, where individual fibers are connected through mechanical interlocking and hydrogen bonds [19, 31]. Despite the complexity, there is a rich history of analyzing the structural properties of paper based on its fiber composition with continuum models [8, 32, 33], with more recent development focusing on, for example, paperboard [2, 37]. These continuum models provide insights into fundamental concepts. However, they are usually limited by a wide range of specialized parameters that are not always accessible to a paper developer in the industry.

A different approach is to simulate the entire microstructure, which involves modeling all the individual paper fibers in the paper product. With this approach, the model parameters are primarily based on the fibers used in the product.

✉ Morgan Görtz  
morgan.gortz@fcc.chalmers.se

<sup>1</sup> Computational engineering and design, Fraunhofer-Chalmers Research Centre for Industrial Mathematics, Chalmers Science Park, Gothenburg 412 88, Sweden

<sup>2</sup> Mathematical Sciences, Chalmers University of Technology and University of Gothenburg, Chalmers tvärgata 3, Gothenburg 412 58, Sweden

<sup>3</sup> Stora Enso, Sommargatan 101, Karlstad 656 37, Sweden

These micro-mechanical models require properties of the individual cellulose fibers [10, 11, 21, 45] and the fiber-fiber interactions in the material [19, 22, 34]. Early simulations with micro-mechanical models evaluated structural properties on sparse network structures [16, 18, 26, 38] using linear beam models, with recent research analyzing the forming of paper products [6, 23, 42], and accurate failure mechanics [3, 43, 44].

Modern micromechanical paper models capture more details but require more computational power to evaluate. Instead of adding complexity, [14] re-evaluated a simple approach similar to [16], with a dimension reduction as in [1], on sheets of lightweight paper. This re-evaluation compared simulated results, experimental results, and theoretical identities for papers composed entirely of a kraft pulp. This article continues that work with the standard Timoshenko model proposed by [26] with heavier, commercial-grade paperboard composed of both CTMP and kraft pulp.

The paperboard models considered in this work are composed of millions of beams, with the dimension of the largest linear system exceeding 100 million degrees of freedom ( $400 \text{ g/m}^2$ ,  $50 \text{ mm} \times 4 \text{ mm}$ , pure kraft). These models require extensive amounts of memory to solve using direct linear solvers, so memory-efficient linear solvers such as iterative methods are preferable. Standard iterative methods require the matrices in these systems to be well-conditioned, which these types of beam models are notoriously not [7]. This hurdle can be overcome using a well-chosen preconditioner [39] that transforms the problem into a well-conditioned system. Whereas several preconditioning approaches exist for models posed on continuums [25, 47], few approaches exist for the discrete network models considered in this work.

Recently [15], a preconditioner for the conjugate gradient method for network models was developed, mathematically motivated, and numerically validated for the network models used in [14]. This preconditioner was inspired by the domain decomposition approach for elliptic problems on continuums [25]. This method divides the model into smaller sub-problems using a finite element grid. These smaller micro-mechanical problems can be solved trivially in parallel, and the method is well suited for computational clusters. Here, the memory efficiency of the method is utilized to solve large-scale problems, which with a direct solver would require specialized hardware. Moreover, this article presents the numerical validation of the method for structural network models based on Timoshenko beams.

This work simulates tensile and bending stiffness experiments of paperboards consisting of an unbleached sulfate kraft pulp and CTMP presented in [5]. These experiments were performed on various three-ply paperboards consisting of layers with different pulps, and in this work, these experiments are re-evaluated digitally using the micro-mechanical model.

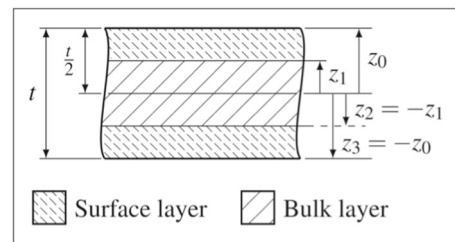


**Fig. 1** An overview of the three-ply paperboards considered in this work, along with ply coordinates  $z_k$  and board thickness  $t$

**Table 1** Experimental data provided in [5]

Sheet properties	Kraft	CTMP
Grammage	400 g/m <sup>2</sup>	400 g/m <sup>2</sup>
Density ( $\rho_s$ )	770 kg/m <sup>3</sup>	423 kg/m <sup>3</sup>
Tensile stiff. MD ( $E_S^{\text{MD}}$ )	10.4 GPa	2.79 GPa
Tensile stiff. CD ( $E_S^{\text{CD}}$ )	2.46 GPa	0.423 GPa
Tensile stiff. effective ( $E_S^*$ )	6.43 GPa	1.61 GPa

The paper starts by introducing the paperboards considered, followed by the presentation of the micro-mechanical model. With the model defined, the iterative numerical method [15] is formulated. Then, the setups of the micro-mechanical simulations are introduced, along with how the results are evaluated. The results are split into three parts: (1) simulations using a direct linear solver on  $200 \text{ g/m}^2$  paperboards, (2) numerical evaluation of using a direct linear solver and convergence analysis of the iterative method in [15], (3) simulations of  $400 \text{ g/m}^2$  paperboard models requiring an iterative approach to be performable on non-specialized hardware (2024). All of the results in this article can be performed on a consumer-grade desktop computer (AMD Ryzen 9 3900X 12-Core, 128GB RAM).

## 2 Three-ply paperboard

Tensile and bending stiffness for three-ply paperboards are simulated and compared to the experimental results in [5]. The boards have a surface weight (grammage) of  $400 \text{ g/m}^2$  and are symmetric in structure with two surface layers and one bulk layer. Figure 1 presents the cross-sectional geometry of the paperboards. The surface layers are composed of kraft pulp, and the bulk is composed of CTMP. The sheets in [5] have orthotropic properties due to fiber bias in the material (machine-direction, MD, and cross-direction, CD). Table 1 presents the experimental results in [5] for boards composed of a single ply that are used to build the models.

### 2.1 Multi-laminar stiffness

The tensile stiffness of layered materials, such as the three-ply paperboards considered, can be estimated using the associated rule of mixtures. In this case:

$$E_{\text{Sheet}} = E_{\text{CTMP}} \frac{t_{\text{CTMP}}}{t} + E_{\text{kraft}} \frac{t_{\text{kraft}}}{t}, \tag{1}$$

where  $t$  is the thickness of the paperboard,  $t_{\text{CTMP}}$  is the thickness of the layer composed of CTMP, and  $t_{\text{kraft}}$  is the combined thicknesses of the two surface layers composed of kraft.

Paper bending stiffness,  $S_b$ , is defined as:

$$S_b = \frac{EI}{w} = \frac{Et^3}{12},$$

where  $E$  is the Young’s modulus,  $I$  the second moment of area,  $w$  the width, and  $t$  is the thickness of the paper. This stiffness is useful because it can be calculated without having the thickness of the paper.

The theoretical bending stiffness of multi-layered paperboard was presented and validated experimentally in [5]. For three-ply paperboard, the following scaling was proposed:

$$S_b = D - \frac{B^2}{A}, \tag{2}$$

$$A = \sum_{k=1}^3 (E_S)_k (z_k - z_{k-1}),$$

$$B = \frac{1}{2} \sum_{k=1}^3 (E_S)_k (z_k^2 - z_{k-1}^2),$$

$$D = \frac{1}{3} \sum_{k=1}^3 (E_S)_k (z_k^3 - z_{k-1}^3),$$

where  $(E_S)_k$  is the associated tensile stiffness of the  $k$ :th ply and the ply-coordinates,  $z_k$ , are defined as:

$$z_k = \begin{cases} -t/2, & k = 0, \\ z_{k-1} + t_k, & \text{else,} \end{cases}$$

where  $t$  is the thickness of the paperboard and  $t_k$  is the thickness of the  $k$ :th ply. For an illustration of the ply coordinates  $z_k$  for a three-ply paperboard, see Fig. 1.

### 3 Micro-mechanical model

A paper-based material is composed of paper fibers. The proposed method models each fiber as several connected one-

Fig. 2 Illustration of the projected length (dotted line) of a fiber (black). The dashed circle is the smallest circle that contains the fiber



dimensional beams in a spatial network model. The bonds between fibers are also modeled as beams. All beams are linear Timoshenko beams [26] with parameters motivated by micro-scale experiments and established constitutive relations used to evaluate various properties of paper.

All except three of the micro-mechanical model parameters are *uniquely* determined by experiments or constitutive relations, with two of them being related to bonding. The first of the three exceptions is the cell wall thickness of the fibers, the second is Young’s modulus of the bonds, and the third is the cross-section of the beams representing the bonds. Instead of fitting these parameters to get anticipated results, the values are taken from experiments to show how close the predictions are without the need for fitting.

The micro-scale model is introduced by first describing the methodology of discretizing, placing, and connecting (bonding) the fibers. Then, the constitutive beam model is presented for the beams in the model, followed by the micro-mechanical parameters used. For an overview of the properties, see Tables 2 and 3.

#### 3.1 Network generation

Figure 1 presents the cross-section of the three-ply paperboards considered. A specified board width, length, weight, and coarseness define how many fibers are placed in each layer. Each fiber shape is generated stochastically based on the geometrical distribution from pulp experiments and deduced properties presented in Tables 2 and 3.

The curvature of a fiber is defined by the experimental distributions of arc length and shape factor using the following relation:

$$\text{shape factor} = \frac{\text{projected length}}{\text{arc length}},$$

where length and projected length are specified in Fig. 2. The curvature of the fiber is implemented by giving the fiber a cosine or sine shape with 0.5 to 2 periods based on the shape factor of the fiber.

The fibers are modeled as chains of 0.1 mm Timoshenko beams and placed stochastically and periodically in the plane of the model, with a small random rotation out of the plane (from horizontal to approximately twice the thickness of a fiber). The in-plane angle of the fibers,  $\gamma$ , has to be biased for the micro-mechanical model to have orthotropic properties.

For the kraft fibers, it is possible to get an associated cos-1 probability density function (PDF) (4) of the orientations of the fibers in the network based on the orthotropy of the sheet [8]:

$$3.73 \approx \frac{E_{\text{kraft}}^{\text{MD}}}{E_{\text{kraft}}^{\text{CD}}} = \frac{6 + 4\eta}{6 - 4\eta} \Leftrightarrow \eta \approx 0.865. \quad (3)$$

$$f_{\eta}^{\text{cos1}}(\gamma) = \frac{1}{\pi} (1 + \eta \cos(2\gamma)), \quad \gamma \in \left[-\frac{\pi}{2}, \frac{\pi}{2}\right]. \quad (4)$$

For straight fibers, the cos-1 distribution can be used directly. To account for the curvature of the fibers, the following weighted version of the cos-1 distribution,  $f_{\eta,s}(\gamma)$ , is used when placing the fibers:

$$\begin{aligned} f_{\eta,s}(\gamma) &= \frac{\hat{f}_{\eta,s}(\gamma)}{\int_{-0.5\pi}^{0.5\pi} \hat{f}_{\eta,s}(\gamma) d\gamma}, \quad \gamma \in \left[-\frac{\pi}{2}, \frac{\pi}{2}\right] \\ \hat{f}_{\eta,s}(\gamma) &= f_{\eta}^{\text{cos1}}(\gamma) f_s^{\text{normal}}(\gamma), \\ f_s^{\text{normal}}(\gamma) &= \frac{1}{s\sqrt{2\pi}} \exp(-0.5(\gamma/s)^2). \end{aligned} \quad (5)$$

By generating networks with curved kraft fibers and computing the orientation distribution, which is based on fiber segments, it was found that  $\eta = 1$ ,  $s = 0.8$  produce a good match corresponding to  $f_{0.865}^{\text{cos1}}$ , (3), (4), for straight fibers.

Similarly, using (3) for the CTMP fibers gives an  $\eta = 1.06$ , which is outside the scope of cos-1 (the PDF becomes negative). Instead, the choice of distribution for the CTMP fibers was determined by testing different  $f_{\eta,s}(\gamma)$  to reproduce the experimental tensile stiffness of sheets composed solely of CTMP. With this approach,  $f_{1,0.6}(\gamma)$  was found to be a good match and is used for the CTMP fibers.

Using a stochastic approach to place fibers will lead to overlaps. A more realistic approach would be to simulate the laydown process [23, 42] or to simulate compaction [6]. Here, randomization was used for simplicity, especially considering the scales of the problems considered.

With fiber shapes and positions generated in each of the three layers, the fibers are connected (bonded). The bonding is based on the three-dimensional volume of the fibers. If any two types of fibers intersect, the intersection region is found between the two fibers. This region is then discretized by placing nodes with a fixed distance along the two fibers in the region. These nodes are then connected by beams with circular cross-sections with area  $30 \mu\text{m}$  times the region discretized, where  $30 \mu\text{m}$  is a typical fiber width. These beams are isotropic with Young's modulus  $0.5(E_f^{\text{CTMP}} + E_f^{\text{kraft}})$ . The discretization distance was chosen to be  $0.075 \text{ mm}$ , as further discretization led to minimal change in the simulation results. Figure 3 presents an illustration of this bonding process.

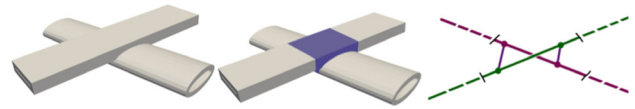


**Fig. 3** The left figure shows parts of two fibers that intersect, with the middle picture highlighting the intersection. The right figure presents the network model representation of the intersection, with two bonds added that discretize the intersecting region

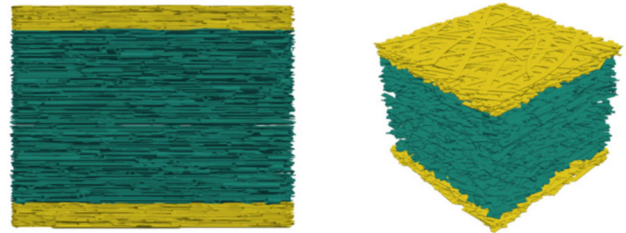


**Fig. 4** Cross-section (left) and overview (right) of a  $1 \text{ mm} \times 1 \text{ mm}$ ,  $400 \text{ g/m}^2$  paper model with  $1/3$  of the mass in the surface layers (kraft) and  $2/3$  of the mass in bulk (CTMP). The fibers are colored to illustrate the three layers, with yellow for the surface layers (kraft) and green for the bulk (CTMP). Note that the weight distribution is not the same as the volume distribution

With the network bonded, the largest connected subnetwork is found, and all components not connected to this network are removed. This step is necessary to make the system solvable, as periodically placing fibers can result in tiny disconnected parts of fibers on the boundaries. Figure 4 presents the cross-section of a generated three-ply paper model.

### 3.2 Constitutive model

The beams representing the paper fibers and bonds are modeled using the linear Timoshenko model proposed in [26] for paper materials. In the linear Timoshenko framework, each node  $i$  in the network is described by six degrees of freedom:  $[\mathbf{u}^i, \boldsymbol{\phi}^i] = [u_x^i, u_y^i, u_z^i, \phi_x^i, \phi_y^i, \phi_z^i]$ , with  $\mathbf{u}^i$  representing the displacement and  $\boldsymbol{\phi}^i$  the rotation in the corresponding network node.

For each beam, say between node  $i$  and  $j$ , in the network, a linear relationship between the twelve degrees of freedom of the two nodes,  $(\mathbf{u}^i, \boldsymbol{\phi}^i, \mathbf{u}^j, \boldsymbol{\phi}^j)$ , is mapped to directional forces and moments resulting from the displacement as follows:

$$K_{ij} \begin{bmatrix} \mathbf{u}^i \\ \boldsymbol{\phi}^i \\ \mathbf{u}^j \\ \boldsymbol{\phi}^j \end{bmatrix} = \begin{bmatrix} \mathbf{F}^i \\ \mathbf{M}^i \\ \mathbf{F}^j \\ \mathbf{M}^j \end{bmatrix},$$

where  $[\mathbf{F}^\star, \mathbf{M}^\star] = [F_x^\star, F_y^\star, F_z^\star, M_x^\star, M_y^\star, M_z^\star]$ , for  $\star = i, j$ .

The linear relation, or stiffness contribution, can be defined by [7]:

$$K_{ij} = l_{ij} Q_{ij}^T (B_{ij}^T C_{ij} B_{ij}) Q_{ij},$$

where  $l_{ij}$  is the length of the beam,  $Q_{ij} \in \mathbb{R}^{12 \times 12}$  is an orthogonal matrix mapping the beam's initial direction to a reference configuration (beam along the  $x$ -axis, the two perpendicular axes aligned with the  $y$ - and  $z$ -axis),  $B_{ij} \in \mathbb{R}^{6 \times 12}$  contains the structure of the relation dependant on the length of the beam, and  $C_{ij} \in \mathbb{R}^{6 \times 6}$  is a diagonal matrix with the beam's structural parameters. The six diagonal elements of  $C_{ij}$  are  $[E_f A^{ij}, kG_f^t A^{ij}, kG_f^t A^{ij}, G_f I_x^{ij}, E_f^t I_y^{ij}, E_f^t I_z^{ij}]$ . Of these,  $E_f, E_f^t$  are the axial and transversal elastic modulus of the specific beam. The shear moduli of the beams are chosen as for isotropic beams with Poisson's ratio  $1/3$ ,  $G = 3E/8$ , with associated Young's modulus  $E$ . Cross-section area ( $A^{ij}$ ) and the second moment of areas ( $I^{ij}$ ) are calculated based on the cross-section geometry of the beam. The shear correction factor  $k$  is chosen according to Cowper selection for a circular cross-section with Poisson's ratio  $1/3$ ,

Adding all of these stiffness contributions from each beam in the network together into one global system results in the following linear system:

$$K \begin{bmatrix} \mathbf{u} \\ \boldsymbol{\phi} \end{bmatrix} = \begin{bmatrix} \mathbf{F} \\ \mathbf{M} \end{bmatrix}, \tag{6}$$

$$\mathbf{u} = [\mathbf{u}^1, \mathbf{u}^2, \dots, \mathbf{u}^n]^T, \mathbf{F} = [\mathbf{F}_1, \mathbf{F}_2, \dots, \mathbf{F}_n]^T,$$

$$\boldsymbol{\phi} = [\boldsymbol{\phi}^1, \boldsymbol{\phi}^2, \dots, \boldsymbol{\phi}^n]^T, \mathbf{M} = [\mathbf{M}_1, \mathbf{M}_2, \dots, \mathbf{M}_n]^T.$$

The stiffness matrix,  $K$ , in (6) can be used to construct linear systems to analyze a paper's structural properties. In this work, linear systems are created and solved with explicitly imposed boundary conditions depending on the specific structural simulation.

### 3.3 Model parameters

Experimental measurements define the weight, length, width, and shape of the individual fibers in the model. These measurements were performed by Stora Enso in 2020, using L&W's Fiber Tester Plus on two pulps. Table 2 presents the results from these measurements for the two pulps: an unbleached sulfate kraft pulp and a CTMP. Mean results for the pulp, such as coarseness (weight per unit length) and measurements for five specific fiber length intervals, are provided. The coarseness of the kraft pulp is lower than the CTMP, with the fibers from the CTMP generally being shorter and wider. This fiber analysis provides most of the geometric information necessary to model representative fibers from

each pulp but does not provide information about the fibers' cross-section area.

For the cross-section area, the linear relation  $A_f = c_f / \rho_f$  is assumed where  $A_f$  is the cross-section area (without lumen),  $c_f$  is the coarseness of the fiber, and  $\rho_f = 1500 \text{ kg/m}^3$  is the density of cellulose. This means that the cross-section areas of the kraft pulp are  $131 \mu\text{m}^2$  and CTMP are  $202 \mu\text{m}^2$ . The linear relation is consistent with the experimental measurements performed by [21]. In [4, 28], cell-wall thicknesses  $2.36 \mu\text{m}$  and  $4.0 \mu\text{m}$  are proposed for softwood fibers, here, the same constant cell-wall thickness of  $3 \mu\text{m}$  as in [14] is chosen.

Young's moduli of the paper fibers were calculated using constitutive formulas similar to [9]. In [9], they use Cox's formulation [8], which is valid for higher-density paper. Here, both low-density and high-density are considered, so Perkins' formula for tensile stiffness [20] is appropriate:

$$E_s^* = \frac{1}{3} \frac{\rho_s}{\rho_f} \phi_P E_f, \tag{7}$$

where  $E_s^* = 0.5(E_s^{\text{MD}} + E_s^{\text{CD}})$ ,  $E_s^{\text{MD}}$  and  $E_s^{\text{CD}}$  are the stiffness of the sheet in both principle directions,  $\rho_s$  and  $\rho_f$  are the densities of the sheet and cellulose respectively,  $E_f$  is the tensile stiffness of the fiber, and  $\phi_P$  is a constant depending on the average fiber length and the sheet bonds. Interpolating the values in the table in [20] with respect to sheet density gives  $\phi_P^{\text{CTMP}} = 0.813$ . For the kraft sheets, the Cox part is sufficient ( $\phi_P^{\text{kraft}} = 1$ ). The tensile stiffness and density of comparable sheets composed entirely of a groundwood pulp (CTMP) and a chemical pulp (kraft) were measured by [5]. The relevant results are presented in Table 1, and using these values with (7) gives  $E_f^{\text{kraft}} \approx 38 \text{ GPa}$  and  $E_f^{\text{CTMP}} \approx 20 \text{ GPa}$  which will be used as the axial stiffness for the respective fibers in the network models. The transverse modulus of the fibers is  $1/3$  of the tensile stiffness to model the anisotropy of the fibers [10].

### 4 Simulation setups

The tensile and bending stiffness of various three-ply paper-board models is evaluated. In the simulations, the board models have a width of 4 mm, which is deemed sufficient by evaluating wider models that produce similar results. In the tensile stiffness simulations, the models have a 4 mm length which was similarly deemed sufficient. For bending stiffness, models of various lengths are evaluated and analyzed.

In the tensile stiffness simulation, the model is fixed both spatially and rotationally on two opposite sides, with one displaced 0.5% to introduce stress. The equilibrium of the problem is solved, and the resulting internal forces are summed up and used to calculate the tensile stiffness.

**Table 2** Geometrical breakdown of an unbleached kraft pulp and a CTMP, provided by Stora Enso

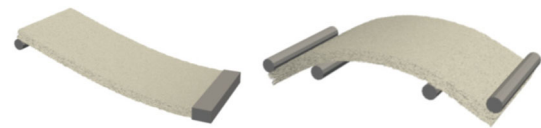
Properties	Kraft	CTMP
Coarseness	196 $\mu\text{g}/\text{m}$	303 $\mu\text{g}/\text{m}$
Mean arc length	2.2 mm	1.7 mm
Mean width	32 $\mu\text{m}$	36.8 $\mu\text{m}$
Mean shape factor	86.8%	88%
Arc length: 0.2–0.5 mm	8.5%	20%
Mean width	22.2 $\mu\text{m}$	25.4 $\mu\text{m}$
Mean shape factor	91.4%	88.1%
Arc length: 0.5–1.5 mm	20.1%	30.2%
Mean width	29.3 $\mu\text{m}$	35.9 $\mu\text{m}$
Mean shape factor	88.8%	88.1 %
Arc length: 1.5–3 mm	45.9%	34.9%
Mean width	32.8 $\mu\text{m}$	40.9 $\mu\text{m}$
Mean shape factor	87.1%	89.3 %
Arc length: 3–4.5 mm	23.5%	13.0%
Mean width	35.6 $\mu\text{m}$	44.1 $\mu\text{m}$
Mean shape factor	83.7%	85.7 %
Arc length: 4.5–7.5 mm	2%	1.9%
Mean width	38.3 $\mu\text{m}$	46.9 $\mu\text{m}$
Mean shape factor	73.6%	78.4 %

**Table 3** Deduced parameters of the fiber models

Properties	Kraft	CTMP
Cross-section area ( $A$ )	131 $\mu\text{m}^2$	202 $\mu\text{m}^2$
Axial modulus ( $E_f$ )	38 GPa	20 GPa
Transverse modulus ( $E_f^t$ )	13 GPa	6.7 GPa
Axial shear modulus ( $G_f$ )	14 GPa	7.5 GPa
Transverse shear modulus ( $G_f^t$ )	4.9 GPa	2.5 GPa
Shear correction factor ( $k$ )	0.89	0.89
Cell wall thickness	3.0 $\mu\text{m}$	3.0 $\mu\text{m}$
Typical cross section	Rectangular	Ellipse

## 4.1 Bending stiffness

For paper products like paper and paperboard, bending stiffness is normalized with Euler–Bernoulli theory. These calculations assume pure bending with no shearing or boundary effects. Long levers are used to mitigate shearing effects, with [30] recommending lever-to-thickness ratios over 40. The thickest 200 g/m<sup>2</sup> paperboard considered is the board composed entirely of CTMP and has a thickness of 0.47 mm. This means that for accurate bending stiffness experiments, a lever of at least 19 mm is suggested. This work simulates two methods to evaluate bending stiffness: the two-point and four-point methods. The two-point method is a common method for evaluating the bending stiffness of paperboard,


**Fig. 5** Illustration of the two (left) and four-point (right) bending stiffness experiments

whereas, for thicker materials with greater anisotropic shear properties (such as porous material and corrugated paperboard), the four-point method can allow representative results for bending-type experiments with smaller bending levers. Figure 5 illustrates the two-point and four-point bending stiffness methods.

The experiments [5] used to validate the bending stiffness simulations used a two-point method. Taking the same approach in the simulation results in a clamped and displaced side. In the experiment, the measurement/displacement probe is free to move along the paper, with only the  $z$ -coordinate locked in the simulation for the displaced nodes. Anisotropic behavior is observed for the choice of bending lever, so multiple levers are simulated and analyzed. The bending stiffness for the model is evaluated as follows [30]:

$$S_b = \frac{F^b l_b^3}{3\delta_b w_b}, \quad (8)$$

where  $F^b$  is the lateral force resulting from the displacement,  $l_b$ ,  $\delta_b$  are the lever and displacement in the two-point method, and  $w_b$  is the width of the paper model.

Four-point bending stiffness experiments are simulated by adding Dirichlet conditions in five planes perpendicular to the bending lever ( $x$ -axis). For beams crossing such a plane, the beam is subdivided and a Dirichlet node is created in the plane. First, a network model is generated in the domain  $[0, l] \times [0, 4 \text{ mm}] \times [0, t]$ , where  $l$  is the length, 4 mm is the width, and  $t$  is the thickness of the paper modeled. The first set of Dirichlet nodes is the two planes at the ends of the paper model. Here, the model is only fixed in the out-of-plane direction to some specified displacement. In the second set of Dirichlet nodes, the planes at  $x = 0.25l$  and  $x = (1 - 0.25)l = 0.75l$  are fixed in the out-of-plane direction. The final plane where Dirichlet nodes are placed is in the middle of the model,  $x = l/2$  where the model is fixed in-plane. No Dirichlet conditions are imposed on the rotational degrees of freedom. The bending stiffness is then evaluated by solving the linear system with the Dirichlet conditions explicitly imposed and using the formula [30]:

$$S_b = \frac{\bar{F}^b (0.25l)(0.5l)^2}{8\delta_b w_b}, \quad (9)$$

where  $\bar{F}^b$  is the average size of the four out-of-plane forces acting on the four planes with out-of-plane Dirichlet conditions and  $\delta_b$  is the average out-of-plane displacement in the center plane with in-plane Dirichlet conditions.

### 5 Domain decomposition

In the largest structural simulations, systems of equations requiring large amounts of primary memory are evaluated. For the full 400 g/m<sup>2</sup> bending simulations, 500GB of primary memory (by swapping to secondary memory) was insufficient for the direct linear solver. To handle these problems with hardware with 128GB of RAM, a different approach is necessary. One such approach is using an iterative solver. Standard iterative solvers typically require the matrices in these problems to be well-conditioned, which these linear network models are not [7]. However, ill-conditioned problems can be transformed into something more appropriate for iterative methods with a well-chosen preconditioning technique.

In [15], a preconditioner based on domain decomposition for the iterative conjugate gradient method was proposed and mathematically motivated for linear network problems similar to those considered in this work. This iterative approach is based on a subspace decomposition into a finite element space, defined on a coarse grid, and overlapping local subspaces, defined for each node in the coarse grid. In each iteration, a single global solve on the finite element grid is made followed by one local solve for each grid point. All these problems can be solved in parallel, which makes the method appropriate for computer clusters.

The ideal choice of the grid is based on the network’s connectivity, homogeneity, and locality, which is generally as fine as possible but where each element contains a well-connected similar-sized network. The finite element grids used in this work are three-dimensional square grids with 1 mm × 1 mm elements in-plane with one element throughout the thickness of the paper model.

The iterative method approximates the solution  $[\mathbf{u}, \boldsymbol{\phi}]$  in (6), by solving a slightly modified problem:

$$K([\mathbf{u}_h, \boldsymbol{\phi}_h]^T + [\mathbf{u}_{g_0}, \boldsymbol{\phi}_{g_0}]^T) = [\mathbf{F}, \mathbf{M}]^T,$$

where  $\mathbf{u}_{g_0}, \boldsymbol{\phi}_{g_0}$  are arbitrary functions that fulfill the Dirichlet conditions. This transforms the problem into:

$$K[\mathbf{u}_h, \boldsymbol{\phi}_h]^T = [\mathbf{F}, \mathbf{M}]^T - K[\mathbf{u}_{g_0}, \boldsymbol{\phi}_{g_0}]^T, \\ [\mathbf{u}, \boldsymbol{\phi}] = [\mathbf{u}_h + \mathbf{u}_{g_0}, \boldsymbol{\phi}_h + \boldsymbol{\phi}_{g_0}],$$

which is a similar problem but has homogeneous Dirichlet conditions, which is required for the method. The

domain decomposition method then finds subsequently better approximations  $[\mathbf{u}_h^{(k)}, \boldsymbol{\phi}_h^{(k)}]$ ,  $k = 1, \dots$  iteratively, where  $\mathbf{u}_h^{(0)} = \boldsymbol{\phi}_h^{(0)} = 0$ , and the approximation to the original problem (6) is  $[\mathbf{u}^{(k)}, \boldsymbol{\phi}^{(k)}] = [\mathbf{u}_h^{(k)} + \mathbf{u}_{g_0}, \boldsymbol{\phi}_h^{(k)} + \boldsymbol{\phi}_{g_0}]$ . The required amount of iterations is dependent on the problem, initial error ( $|\mathbf{u} - \mathbf{u}^{(0)}|$  and  $|\boldsymbol{\phi} - \boldsymbol{\phi}^{(0)}|$ ), and specified convergence condition.

The choices of  $\mathbf{u}_{g_0}, \boldsymbol{\phi}_{g_0}$  are arbitrary, but with this construction, it acts as an initial guess. Here, the guess is based on a one-dimensional Timoshenko-beam representation of the paper sheet. For the tensile stiffness simulations, this means that  $\mathbf{u}_{g_0}$  is the pure linear displacement in the x-coordinate and  $\boldsymbol{\phi}_{g_0} = 0$ .

In the bending stiffness simulations,  $\mathbf{u}_{g_0}, \boldsymbol{\phi}_{g_0}$  is found by interpolating the solution of the simplified continuum model of the sheet. For this, a Timoshenko beam model represents the bend profile of the sheet. The structural parameters of the model are  $E = 5\text{GPa}$  and  $E/G = 50$ , where the shear ratio is taken from the literature [30], and the elastic modulus is between the values presented in [5]. With the solution to the continuum representation ( $[\mathbf{u}^{\text{sheet}}, \boldsymbol{\phi}^{\text{sheet}}]$ ), the approximation  $\mathbf{u}_{g_0}, \boldsymbol{\phi}_{g_0}$  to the fiber-based approach is:

$$\begin{cases} u_{g_0,x}^k = (t/2 - z) \arctan(-\phi_y^{\text{sheet},\tilde{k}}), \\ u_{g_0,z}^k = u_z^{\text{sheet},\tilde{k}}, \quad u_{g_0,y}^k = 0, \\ \phi_{g_0,y}^k = \arctan(\phi_y^{\text{sheet},\tilde{k}}), \quad \phi_{g_0,x}^k = \phi_{g_0,z}^k = 0, \end{cases}$$

where  $[x, y, z]$  is the position of the node  $k$ ,  $t$  is the thickness of the paperboard modeled, and  $u_z^{\text{sheet},\tilde{k}}, \phi_y^{\text{sheet},\tilde{k}}$  is the  $z$ -displacement and  $y$ -rotation in the closest discretization point in the simplified continuum model to the node  $k$ . Figure 5 was constructed by displacing a micro-mechanical paperboard model to  $\mathbf{u}_{g_0}, \boldsymbol{\phi}_{g_0}$  for a two-point and four-point simulation.

### 6 Micro-mechanical simulations

Micro-mechanical simulations in both machine-direction and cross-direction using the network model are compared to the experimental results of [5]. In the experiments, 400 g/m<sup>2</sup> sheets are composed of mechanical and chemical pulp. Both 200 g/m<sup>2</sup> and 400 g/m<sup>2</sup> models are simulated. A direct linear solver is able to solve the 200 g/m<sup>2</sup> models, but the densest paper models hit the computational limit for a computer with 128GB of RAM. A different approach is necessary for the full 400 g/m<sup>2</sup> models. Here, the convergence rate and accuracy for the proposed domain decomposition method are evaluated in detail for these Timoshenko beam models, and using these results, problems surpassing the computational limit of the direct approach are solved.

## 6.1 200 g/m<sup>2</sup> simulations

The experiments in [5] for 400 g/m<sup>2</sup> paperboard models are compared to tensile stiffness simulations on 200 g/m<sup>2</sup> paperboard models. These 200 g/m<sup>2</sup> models are similar to Stora Enso's CKB Nude™ 205 with similar grammage, structure, and pulp. In the experiments [5], the bending stiffness is analyzed with respect to the following weight-fraction:

$$\text{weight fraction} = \frac{\text{weight of surface layers}}{\text{total weight}},$$

where a board with weight fraction 0% is entirely bulk (CTMP), and 100% is one large surface layer (kraft pulp).

Figure 6 and Table 4 presents the experimentally obtained tensile stiffness in [5], rule of mixtures (1), and the tensile stiffness from the micro-mechanical simulation of several different three-ply paperboards with various weight fractions. The stresses on individual fibers in a micro-mechanical tensile stiffness simulation are presented in Fig. 7. The results of these simulations show that the tensile stiffness of papers composed entirely of one pulp is consistent with Perkins' formula for tensile stiffness (7) for kraft pulp, with the micro-mechanical models composed of CTMP predicting 25% stiffer effective tensile stiffness:

$$\frac{E_{\text{kraft, sim}}^*}{E_{\text{kraft, exp}}^*} = 1.054, \quad \frac{E_{\text{CTMP, sim}}^*}{E_{\text{CTMP, exp}}^*} = 1.24.$$

The discrepancy for the CTMP fibers can be removed by choosing a 20% lower  $\phi_P$  when choosing the tensile stiffness for the CTMP fibers.

The orthotropy is captured to a large extent in the model:

$$\frac{\sigma_{\text{kraft, sim}}}{\sigma_{\text{kraft, exp}}} = 0.90, \quad \frac{\sigma_{\text{CTMP, sim}}}{\sigma_{\text{CTMP, exp}}} = 0.84, \quad \sigma_{\star} = \frac{E_{\star}^{\text{MD}}}{E_{\star}^{\text{CD}}},$$

with the model predicting roughly 10% less anisotropy for sheets made of kraft and 15% less for sheets made of CTMP compared to the experiments. The kraft discrepancy can be fixed by using a more weighted orientation distribution, but for sheets composed of CTMP, the orientation distribution of the fibers in the model is already quite extreme. For further orthotropy, it might be necessary to use other fiber shapes than the ones considered in this work.

The non-linear curves in Fig. 6 are calculated based on the tensile stiffness of the paperboards composed entirely of one pulp in both machine and cross-direction. For comparison, both curves derived from the experiments in [5] and the simulated stiffness are presented. The results clearly show that the linear network model captures the anticipated scaling for the evaluated three-ply paperboards.

Figure 8 presents the simulated bending stiffness for the thickest 200 g/m<sup>2</sup> paperboard considered in both principle

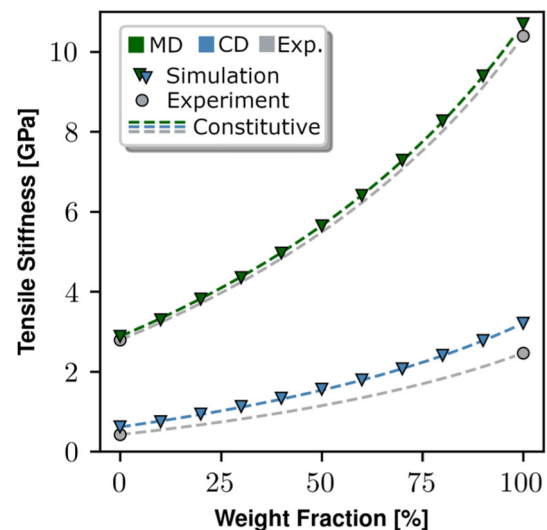


**Fig. 6** Tensile stiffness for 200 g/m<sup>2</sup> three-ply paperboard models with different weight distributions for the surface/bulk layers in both machine-direction and cross-direction. The circular markers are experimental measurements [5], the colored markers are simulated results, and the dashed lines are the rule of mixtures based on the experiments (gray) and simulation (colored)

**Table 4** Selected data, (MD, CD), presented in Fig. 6

W. F	Sim. $E_x$ , GPa	Exp. $E_x$ , GPa
0%	(2.88, 0.614)	(2.46, 0.43)
50%	(5.64, 1.56)	×
100%	(10.7, 3.21)	(10.4, 2.79)

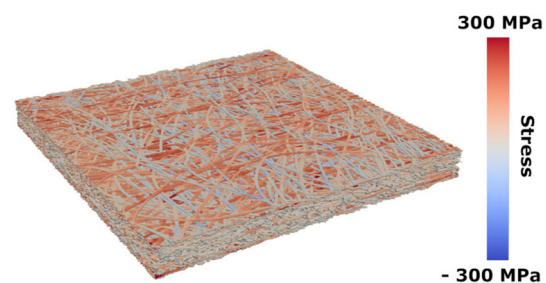


**Fig. 7** An illustration of the solution of a 200 g/m<sup>2</sup> tensile stiffness simulation

directions with varying bending levers by both the two-point and four-point setup. Along with these simulated results, theoretical bending stiffness scaling is calculated using a Timoshenko beam representing the sheet. These beam representations are evaluated with Elastic–Shear modulus ratio ( $E/G$ ) of 50 [30], 130 [46], and 274 [29].

From comparison in Fig. 8, it is clear that the two-point results anticipate a shear ratio on the higher end with a slightly different scaling in the machine-direction. For cross-direction the scaling seems in line with the previous experiments. Differences in the theoretic scaling and scal-



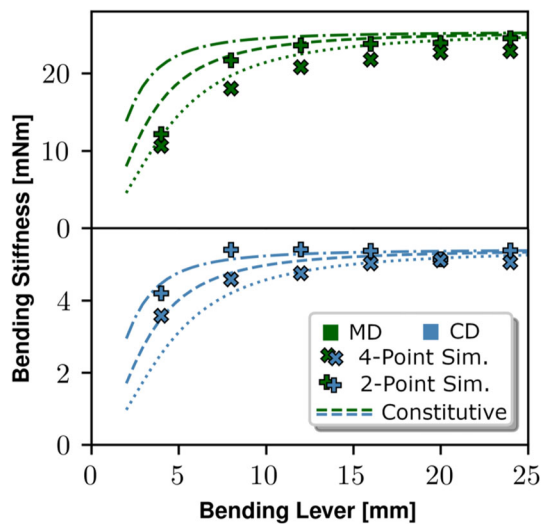


**Fig. 8** Results from two-point and four-point bending stiffness simulations for different bending levers for 200 g/m<sup>2</sup> paperboard composed entirely of CTMP in both principle directions. The dashed lines are predictions based on the simulated tensile stiffness of the sheet using a Timoshenko beam representation of the paper sheet for different tensile/shear stiffness ratios found in the literature

ing observed in experiments are discussed in [30], where experimental results show a similar difference between two- and four-point methods. Here, it is argued that the boundary effects of clamping the paper could be the reason for the discrepancy. The simulated results in this domain study show that a 16 mm bending lever is sufficient for the four-point method, with the two-point simulations having almost converged to the anticipated bending stiffness at 24 mm.

The bending stiffnesses of 200 g/m<sup>2</sup> three-ply paperboards with varying surface layer thickness are evaluated numerically using the linear network model. Two- and four-point methods are evaluated, and the simulated results are compared to the theoretical bending stiffness based on the constitutive Eq. (2), with parameters found experimentally in [5]. The results are presented in Fig. 9 and Table 5 for simulations on the scale 24 mm × 4 mm for the two-point method and 16 mm × 4 mm for the four-point method. From these results, one can observe that the bending stiffness is lower in the machine-direction than predicted by the constitutive formula based on the simulated tensile stiffness but is consistent with the formula in cross-direction. However, with the slightly lower orthotropy, it is clear that the linear network model can predict the quadratic relation between weight fraction and bending stiffness.

### 6.2 Comparison of the linear solvers

The simulations performed for the results in Fig. 9 were solved with a direct linear solver. These simulations are resource intensive; see Table 6. In the case of the two-point

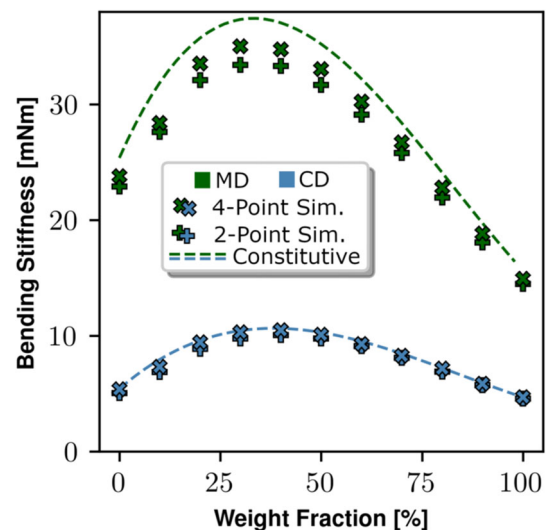


**Fig. 9** Bending stiffness for different weight distributions in various 200 g/m<sup>2</sup> three-ply paperboard. The markers are simulated results, and the dashed lines are calculated using multi-laminar theory using the simulated tensile stiffness for sheets composed of one pulp in Fig. 6

**Table 5** Selected data, (MD, CD), presented in Fig. 9

W. F	Sim. 2-P $S_b$ , mNm	Sim. 4-P $S_b$ , mNm
0%	(22.9, 5.05)	(23.8, 5.37)
50%	(31.7, 9.76)	(33.0, 10.1)
100%	(14.5, 4.57)	(14.9, 4.67)

**Table 6** Numerical metrics for solving three four-point bending stiffness simulations (CD) in Fig. 9

Weight fraction	0 %	50 %	100 %
Nodes ( $10^6$ )	2.3	3.2	4.1
Beams ( $10^6$ )	3.2	4.5	5.8
System dim. ( $10^6$ )	14	19	25
Memory (primary, GB)	42	66	93
Wall-clock (min)	12	22	37

simulations, all but the last three data points (80%, 90%, 100% kraft) required more than 128GB of RAM, at which the utilized computer had to resort to secondary memory for those points. The main reason for the excessive memory consumption is due to using a direct solver to solve the ill-conditioned linear systems. With 128GB of RAM, 30 mm<sup>3</sup> paperboard models is a rough limit when using a direct linear solver.

The experiments performed in [5] evaluate paperboards with twice the grammage, requiring twice the bending lever, which results in roughly four times larger problems. A different approach is necessary to enable these simulations on non-specialized (2024) hardware.

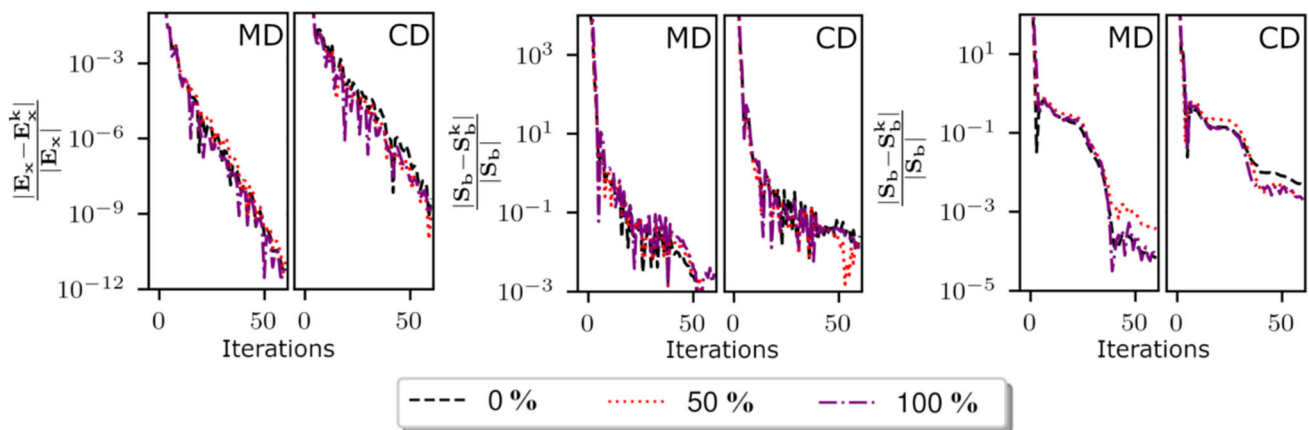


**Fig. 10** Convergence analysis of the iterative solver for three different 200 g/m<sup>2</sup> three-ply paperboards with weight fraction: 0%, 50%, and 100%. This analysis is performed on the tensile stiffness and the two (two-/four-point) bending stiffness simulations. In all figures, the iteration is plotted against the relative error of the structural evaluation

Three 200 g/m<sup>2</sup> paperboards (Figs. 6 and 9) were evaluated using the domain decomposition method. The convergence of the iterative approach is presented in Fig. 10. From these results, we can see that the network structure does not affect the convergence rate, but the iterations in cross-directional simulations have errors about 10 times larger at each iteration compared to the machine-direction counterpart. This is most evident in the cross-directional simulation of the four-point method, where anisotropy compounds the errors to around 40 times larger than in the machine-direction. For tensile stiffness, only ten iterations were required to obtain tensile stiffnesses with a 0.1% difference compared to the direct approach. Similar accuracy for the two-point and four-point bending simulations required 50 iterations for the two-point and 60 iterations for the four-point method. It should be noted that the relative errors of the initial guesses have larger magnitudes in the bending simulations compared to the tensile simulations. Moreover, the algorithm converges to the solution attained using the direct linear solver. Unlike the direct approach, the domain decomposition required, at most, 4.7GB of primary memory per thread for the problems evaluated.

### 6.3 400 g/m<sup>2</sup> simulations

The domain decomposition method can handle far larger problems than the direct approach without running into memory limitations. Here, paperboards of the grammage in [5] are modeled and evaluated. In [5], bending stiffness for paperboards of five weight fractions (0%, 25%, 50%, 75%, and 100%) were evaluated experimentally, and here, these five types of paperboards will be modeled and evaluated.

compared to using a direct solver. The left figure presents the convergence of the iterative method for the tensile stiffness simulations presented in Fig. 6. The center plot is the convergence of the two-point, the right plot the four-point, simulation presented in Fig. 9

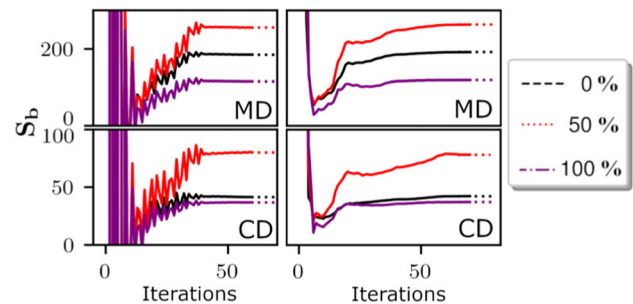


**Fig. 11** Bending stiffness for individual iterates in the domain decomposition method for three of the five full 400 g/m<sup>2</sup> paperboard models. The two left figures present the bending stiffness for the iterates in the two-point simulations, and the right two present the bending stiffness in the four-point simulations. The dashed lines are the converged values

Simulating the tensile stiffness of the 400 g/m<sup>2</sup> paperboard models is less resource intensive than performing the two-point bending stiffness simulations on the 200 g/m<sup>2</sup> paperboards in Fig. 9. Figure 12 presents the tensile stiffness for the five 400 g/m<sup>2</sup> paperboard models in both principle directions solved using a direct linear solver. These results are practically identical to the 200 g/m<sup>2</sup> tensile evaluations in Fig. 6.

Twice the bending levers are necessary when simulating the bending stiffness of the full 400 g/m<sup>2</sup> compared to the 200 g/m<sup>2</sup> models, and this would mean 48 mm levers for the two-point method and 32 mm for the four-point method. In the bending stiffness experiments in [5], the two-point method was performed with a 50 mm lever, and here, the full 50 mm lever is simulated for the two-point method. The four-point method is simulated with a 32 mm lever.

**Fig. 12** Replicated experimental results in [5] (re-drawn) with micro-scale fiber-based simulations of five types of 400 g/m<sup>2</sup> three-ply paperboards. The colored markers and lines are found through simulation, and the gray markers and lines are the experimental results in [5]. The left figure presents the tensile stiffness results, and the right figure presents the bending stiffness results, which was only possible with the domain decomposition method

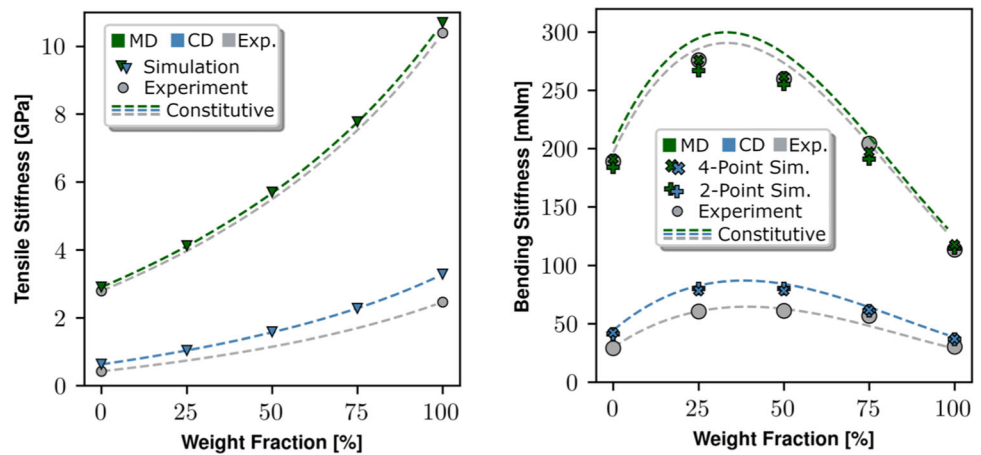


**Table 7** The values, (MD, CD), of the data points in Fig. 12

W. F	Exp. $E_x$ , GPa	Sim. $E_x$ , GPa	Exp. $S_b$ , mNm	Sim. 2-P $S_b$ , mNm	Sim. 4-P $S_b$ , mNm
0 %	(2.46,0.423)	(2.90,0.628)	(189,29.2)	(184,41.3)	(191,42.2)
25%	×	(4.12,1.04)	(276,60.6)	(267,80.1)	(276,78.2)
50%	×	(5.69,1.58)	(260,61.1)	(255,80.1)	(262,78.1)
75%	×	(7.77,2.27)	(204,56.9)	(191,61.2)	(197,61.7)
100%	(10.4,2.79)	(10.7,3.28)	(114,30.6)	(115,36.6)	(118,37.0)

These models are gigantic compared to the 200 g/m<sup>2</sup> counterparts that were pushing the limit with a direct approach, and because of this, only the iterative domain decomposition method is used. The lack of an exact reference solution means that unlike the 200 g/m<sup>2</sup> example in Fig. 10, it is not possible to calculate the exact state of convergence in 400 g/m<sup>2</sup> simulations. Instead, the bending stiffnesses are analyzed with the convergence results in Fig. 10 in mind.

Figure 11 presents the bending stiffness of individual iterates for both the two-point and four-point simulations for three of the five paperboards evaluated. From these results, the bending stiffness seems to converge at around 50 iterations for the two-point method and 60 iterations for the four-point method, similar to the convergence analysis in Fig. 10. This invariance of larger domain sizes of the model is consistent with the theory in [15]. For good measure, 60 iterations were performed for the two-point method, and 70 iterations were performed for the four-point method, at which point minimal changes to the bending stiffness were observed between iterations.

Figure 12 and Table 7 present the bending stiffness for the evaluated five 400 g/m<sup>2</sup> paperboards. The relative difference between the theoretical scaling and the two-point and four-point simulation is similar to the 200 g/m<sup>2</sup> results in Fig. 9, with the cross-directional bending stiffness being consistent with the constitutive equation based on simulated tensile stiffness, and the machine-directional bending stiffness being slightly lower than the constitutive prediction. Unlike the 200 g/m<sup>2</sup>, the bending stiffnesses of the sheets simulated

were experimentally evaluated in [5]. Comparing the simulations with the experiments shows that the simulation produces similar results to those in [5], with cross-direction simulations being slightly stiffer than the experiments, as in the tensile stiffness simulations. Interestingly, the experimental values in the machine-direction seem slightly lower than the constitutive prediction, but this could be because of variance in the experiment. Overall, it is surprising how close the predictions of the micro-mechanical models are, considering the pulp scans are not of the exact pulps used in the experiments [5], the model considered is linear, and there is no fitting in the model.

## 7 Summary and conclusion

Three-ply paperboards consisting of CTMP and kraft pulp are simulated in both principal directions, with the shape of each paper fiber in the model based on detailed pulp analysis and deduced parameters. First, the mechanical parameters of the fibers from each pulp were deduced from the tensile experiments presented by [5] using Perkins' formula for tensile stiffness [20]. Then, tensile stiffness and bending stiffness simulations on various three-ply paperboards showed that the network model was consistent with the experiments and multi-laminar theory that [5] presented.

Out-of-plane micro-mechanical simulations of paperboard have been limited [41], with compaction simulations and out-of-plane responses [6, 27] analyzed on smaller

scales. In this work, the bending stiffness is evaluated on far larger models, and it is shown that linear models can predict the expected theoretical and experimental bending stiffness and tensile stiffness. It would be interesting to evaluate the shear ratio,  $G/E$ , for network generation techniques other than randomization [6, 23, 42].

Simulations of paperboard models with volumes around  $30\text{mm}^3$  were possible with a direct solver, whereas larger models required an alternative approach. Iterative approaches that can solve these Timoshenko beam models require special consideration because of how ill-conditioned the systems are [7]. The iterative method proposed in [15] was numerically validated for these types of systems and used to push the computational limit for network models on consumer-grade hardware accessible to a paper product developer. Moreover, the method is trivially parallelizable and well-suited for computational clusters.

Several optimization techniques could be used to improve the domain decomposition method. Currently, an algebraic version of the network theory used to motivate the method in [15] is being developed [17], and an algebraic version of the iterative method could mean substantial improvements in efficiency. With a more efficient version of the solver, it would be interesting to see how well the domain decomposition approach can handle simulations where multiple linear systems are solved in succession, for example, network models based on non-linear Simo-Reissner beams [36, 40].

Using the same theoretical framework as the iterative domain decomposition method in [15], the theory for a multi-scale method has been developed [12, 24]. This method finds approximations to the micro-scale problem by constructing a representative finite element-inspired coarse scale. With periodicity on some representative element scale in the model, efficient fiber-based simulations should be possible on the scale of A4 sheets.

**Acknowledgements** This work is a part of the ISOP (Innovative Simulation of Paper) project, which is performed by a consortium consisting of Albany International, Stora Enso, and Fraunhofer-Chalmers Centre. The Swedish Foundation for Strategic Research (SSF) supports the first author, and the Swedish Research Council supports the second and third authors in Project Number 2023-03258 VR. The second author was supported by The Åforsk Foundation research Grant 22-166: "Development of simulation tools for bending and fracture propagation of fiber based materials". For efficiency during development, some computations were enabled by resources provided by Chalmers e-Commons at Chalmers.

**Funding** Open access funding provided by Chalmers University of Technology.

## Declarations

**Conflict of interest** The authors declare no conflict of interest.

**Open Access** This article is licensed under a Creative Commons Attribution 4.0 International License, which permits use, sharing, adaptation, distribution and reproduction in any medium or format, as long as you give appropriate credit to the original author(s) and the source, provide a link to the Creative Commons licence, and indicate if changes were made. The images or other third party material in this article are included in the article's Creative Commons licence, unless indicated otherwise in a credit line to the material. If material is not included in the article's Creative Commons licence and your intended use is not permitted by statutory regulation or exceeds the permitted use, you will need to obtain permission directly from the copyright holder. To view a copy of this licence, visit <http://creativecommons.org/licenses/by/4.0/>.

## References

- Adriaenssens S, Barnes M (2001) Tensegrity spline beam and grid shell structures. *Eng Struct* 23(1):29–36
- Borgqvist E, Wallin M, Ristinmaa M et al (2015) An anisotropic in-plane and out-of-plane elasto-plastic continuum model for paperboard. *Compos Struct* 126:184–195. <https://doi.org/10.1016/j.compstruct.2015.02.067>
- Borodulina S, Kulachenko A, Galland S et al (2012) Stress-strain curve of paper revisited. *Nord Pulp Paper Res J* 27(2):318–328. <https://doi.org/10.3183/NPPRJ-2012-27-02-p318-328>
- Borodulina S, Motamedian H, Kulachenko A (2018) Effect of fiber and bond strength variations on the tensile stiffness and strength of fiber networks. *Int J Solids Struct* 154:19–32. <https://doi.org/10.1016/j.ijsolstr.2016.12.013>
- Carlsson LA, Fellers CN (1980) Flexural stiffness of multi-ply paperboard. *Fiber Sci Technol* 13(3):213–223
- Ceccato C, Brandberg A, Kulachenko A et al (2021) Micro-mechanical modeling of the paper compaction process. *Acta Mech* 232(9):3701–3722. <https://doi.org/10.1007/s00707-021-03029-x>
- Cook R, Malkus D, Plesha M et al (2002) Concepts and applications of finite element analysis, 4th edn. Wiley, New York
- Cox HL (1952) The elasticity and strength of paper and other fibrous materials. *Br J Appl Phys* 3(3):72. <https://doi.org/10.1088/0508-3443/3/3/302>
- Czibula C, Brandberg A, Cordill MJ et al (2021) The transverse and longitudinal elastic constants of pulp fibers in paper sheets. *Sci Rep*. <https://doi.org/10.1038/s41598-021-01515-9>
- Czibula C, Seidlhofer T, Ganser C et al (2021) Longitudinal and transverse low frequency viscoelastic characterization of wood pulp fibers at different relative humidity. *Materialia*. <https://doi.org/10.1016/j.mtla.2021.101094>
- Dauer M, Wolfbauer A, Seidlhofer T et al (2021) Shear modulus of single wood pulp fibers from torsion tests. *Cellulose* 28(12):8043–8054. <https://doi.org/10.1007/s10570-021-04027-x>
- Edelvik F, Görtz M, Hellman F et al (2024) Numerical homogenization of spatial network models. *Comput Methods Appl Mech Eng* 418:116593. <https://doi.org/10.1016/j.cma.2023.116593>
- Furszyfer Del Rio DD, Sovacool BK, Griffiths S et al (2022) Decarbonizing the pulp and paper industry: a critical and systematic review of sociotechnical developments and policy options. *Renew Sust Energ Rev*. <https://doi.org/10.1016/j.rser.2022.112706>
- Görtz M, Kettl G, Mållqvist A et al (2022) Network model for predicting structural properties of paper. *Nord Pulp Paper Res J* 37(4):712–724. <https://doi.org/10.1515/npprj-2021-0079>
- Görtz M, Hellman F, Mållqvist A (2024) Iterative solution of spatial network models by subspace decomposition. *Math Comput* 93(345):233–258. <https://doi.org/10.1090/mcom/3861>
- Hamlen RC (1991) Paper structure, mechanics, and permeability: computer-aided modeling. Ph.D. thesis, University of Minnesota

17. Hauck M, Maier R, Målqvist A (2023) An algebraic multi-scale method for spatial network models. [arXiv:2312.09752](https://arxiv.org/abs/2312.09752). arXiv 10.48550
18. Heyden S (2000) Network modelling for evaluation of mechanical properties of cellulose fibre fluff. Ph.D. thesis, LTH
19. Hirn U, Schennach R (2015) Comprehensive analysis of individual pulp fiber bonds quantifies the mechanisms of fiber bonding in paper. *Sci Rep*. <https://doi.org/10.1038/srep10503>
20. Hollmark H, Perkins RW, Andersson H (1978) Mechanical properties of low density sheets. *TAPPI* 61(9):69–72
21. Horn AR (1974) Morphology of wood pulp fiber from softwoods and influence on paper strength. Tech. rep., U.S. Department of Agriculture Forest Service
22. Hubbe M (2006) Bonding between cellulosic fibers in the absence and presence of dry-strength agents—a review. *BioResources*. <https://doi.org/10.15376/biores.1.2.281-318>
23. Kettil G (2019) Multiscale methods for simulation of paper making. Ph.D. thesis, Chalmers University of Technology and University of Gothenburg
24. Kettil G, Målqvist A, Mark A et al (2020) Numerical upscaling of discrete network models. *BIT Numer Math* 60(1):67–92. <https://doi.org/10.1007/s10543-019-00767-2>
25. Kornhuber R, Yserentant H (2016) Numerical homogenization of elliptic multiscale problems by subspace decomposition. *Multiscale Model Simul* 14:1017–1036. <https://doi.org/10.1137/15M1028510>
26. Kulachenko A, Uesaka T (2012) Direct simulations of fiber network deformation and failure. *Mech Mater* 51:1–14. <https://doi.org/10.1016/j.mechmat.2012.03.010>
27. Li Y, Yu Z, Reese S et al (2018) Evaluation of the out-of-plane response of fiber networks with a representative volume element model. *Tappi* 17:325–334. <https://doi.org/10.32964/TJ17.06.329>
28. Lorbach C, Hirn U, Kritzing J et al (2012) Automated 3D measurement of fiber cross section morphology in handsheets. *Nord Pulp Paper Res J* 27(2):264–269. <https://doi.org/10.3183/npprj-2012-27-02-p264-269>
29. Marin G, Srinivasa P, Nygård M et al (2021) Experimental and finite element simulated box compression tests on paperboard packages at different moisture levels. *Packag Technol Sci* 34(4):229–243. <https://doi.org/10.1002/pts.2554>
30. Mark RE, Habeger C, Borch J et al (2002) Handbook of physical testing of paper, vol 1, 2nd edn. Dekker, New York
31. Orgéas L, Dumont P, Martoña F et al (2021) On the role of fibre bonds on the elasticity of low-density papers: a micro-mechanical approach. *Cellulose* 28(15):9919–9941. <https://doi.org/10.1007/s10570-021-04098-w>
32. Page DH (1969) A theory for the tensile strength of paper. *TAPPI* 52:674–681
33. Perkins RW, Mark RE (1976) On the structural theory of the elastic behavior of paper. *TAPPI* 59(12):118–120
34. Persson BNJ, Ganser C, Schmied F et al (2013) Adhesion of cellulose fibers in paper. *J Condens Matter Phys*. <https://doi.org/10.1088/0953-8984/25/4/045002>
35. Pettersson G, Norgren S, Engstrand P et al (2021) Aspects on bond strength in sheet structures from TMP and CTMP—a review. *Nord Pulp Paper Res J* 36(2):177–213. <https://doi.org/10.1515/npprj-2021-0009>
36. Reissner E (1981) On finite deformations of space-curved beams. *Z Angew Math Phys* 32:734–744
37. Robertsson K, Wallin M, Borgqvist E et al (2021) A rate-dependent continuum model for rapid converting of paperboard. *Appl Math Model* 99:497–513. <https://doi.org/10.1016/j.apm.2021.07.005>
38. Räsänen V, Alava M, Nieminen R et al (1996) Elastic-plastic behaviour in fibre networks. *Nord Pulp Paper Res J* 11(4):243–248. <https://doi.org/10.3183/npprj-1996-11-04-p243-248>
39. Saad Y (2003) Iterative methods for sparse linear systems, 2nd edn. Society for Industrial and Applied Mathematics, Philadelphia. <https://doi.org/10.1137/1.9780898718003>
40. Simo J (1985) A finite strain beam formulation, the three-dimensional dynamic problem. part i. *Comput Methods Appl Mech Eng* 49(1):55–70. [https://doi.org/10.1016/0045-7825\(85\)90050-7](https://doi.org/10.1016/0045-7825(85)90050-7)
41. Simon JW (2021) A review of recent trends and challenges in computational modeling of paper and paperboard at different scales. *Arch Comput Methods Eng* 28:2409–2428. <https://doi.org/10.1007/s11831-020-09460-y>
42. Svenning E, Mark A, Edelvik F et al (2012) Multiphase simulation of fiber suspension flows using immersed boundary methods. *Nord Pulp Paper Res J* 27(2):184–191. <https://doi.org/10.3183/NPPRJ-2012-27-02-p184-191>
43. Tojaga V, Kulachenko A, Ostlund S et al (2021) Modeling multi-fracturing fibers in fiber networks using elastoplastic timoshenko beam finite elements with embedded strong discontinuities - formulation and staggered algorithm. *Comput Methods Appl Mech Eng*. <https://doi.org/10.1016/j.cma.2021.113964>
44. Tojaga V, Prapavesis A, Faleskog J et al (2023) Continuum damage micromechanics description of the compressive failure mechanisms in sustainable biocomposites and experimental validation. *J Mech Phys Solids*. <https://doi.org/10.1016/j.jmps.2022.105138>
45. Wang G, Shi SQ, Wang J et al (2011) Tensile properties of four types of individual cellulosic fibers. *Wood Fiber Sci* 43(4):353–364
46. Xia QS, Boyce MC, Parks DM (2002) A constitutive model for the anisotropic elastic-plastic deformation of paper and paperboard. *Int J Solids Struct* 39(15):4053–4071. [https://doi.org/10.1016/S0020-7683\(02\)00238-X](https://doi.org/10.1016/S0020-7683(02)00238-X)
47. Xu J, Zikatanov L (2017) Algebraic multigrid methods. *Acta Numer* 26:591–721. <https://doi.org/10.1017/S0962492917000083>

**Publisher's Note** Springer Nature remains neutral with regard to jurisdictional claims in published maps and institutional affiliations.